Journal of proteome research

pubs.acs.org/jpr

Article

Untargeted 2D NMR Metabolomics of [^{13}C-*methyl*]Methionine-Labeled Tumor Models Reveals the Non-DNA Methylome and Provides Clues to Methyl Metabolism Shift during Tumor Progression

Daniel Morvan*,# and Florent Cachin#

Cite This: *J. Proteome Res.* 2022, 21, 940−952

Read Online

ACCESS | Metrics & More | Article Recommendations | Supporting Information

ABSTRACT: For more than a decade, DNA and histone methylations have been the focus of extensive work, although their relationship with methyl group metabolism was overlooked. Recently, it has emerged that epigenetic methylations are influenced by methyl donor nutrient availability, cellular levels of *S*-adenosyl-methionine (SAM), and cytoplasmic methyltransferase activities. SAM-dependent methyltransferases methylate a wide range of targets, from small molecules to proteins and nucleic acids. However, few investigations of the global methylome of tumors have been performed. Here, untargeted NMR metabolomics of two mouse tumor models labeled with [^{13}C-*methyl*]methionine were used to search for the NMR-visible set of cellular methyl acceptors denoted the global methylome. Tumor models were B16 melanoma cell cultures and B16 melanoma tumors, which may be considered as two stages of B16 tumor development. Based on 2D ^{1}H−^{13}C NMR spectra and orthogonal partial least squares discriminant analysis of spectra, our study revealed markedly different global methylomes for melanoma models. The methylome of B16 melanoma cell cultures was dominated by histone methylations, whereas that of B16 melanoma tumors was dominated by cytoplasmic small-molecule methylations. Overall, the technique gave access to the non-DNA methylome. Comparison of tumor models also exhibiting differential expression of aerobic glycolysis provided clues to a methyl metabolism shift during tumor progression.

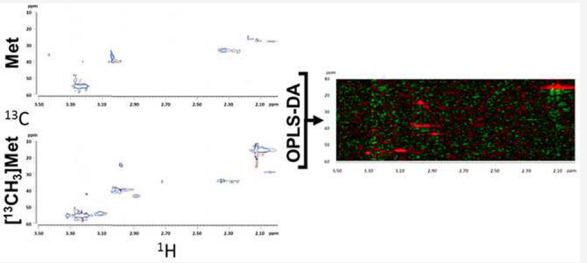

KEYWORDS: *metabolomics, B16 melanoma cell culture, B16 melanoma tumor, L-[^{13}C-methyl]methionine, 2D ^{1}H−^{13}C NMR spectroscopy, high-resolution magic angle spinning, orthogonal partial least squares discriminant analysis, global methylome, methyl metabolism*

INTRODUCTION

Metabolic reprogramming takes place during tumor progression. Aerobic glycolysis, or the Warburg effect, is the combination of increased glucose uptake and elevated lactate production, irrespective of oxygen availability. It is a metabolic hallmark of cancer. Multiple lines of evidence have demonstrated aerobic glycolysis activation by oncogenic signaling pathways during tumor progression.[1] Aerobic glycolysis provides substrates for macromolecular biosyntheses (DNA, lipids, proteins), energy, redox homeostasis, and escape to apoptosis. Recently, it was shown that it also plays a role in tumor microenvironment formation and the epithelial-to-mesenchymal transition.

Other aspects of metabolic reprogramming of tumors include increased glutaminolysis, de novo lipid synthesis, one-carbon metabolism, and others. However, in contrast to aerobic glycolysis, they depend more on the tissue of origin and the prevalence of some cancer-driving mutations.

Another widely shared feature of cancers is aberrant DNA methylation,[2,3] including global hypomethylation and hypermethylation of CpG islands. Hypomethylation is considered to activate proto-oncogenes, while hypermethylation located at gene promoters is associated with silencing of tumor suppressor genes.[3,4] DNA methylation has received extensive attention for more than a decade, along with histone methylation. A number of DNA and histone methylation signatures have been reported in cancer. However, whole-cell methylation of tumor cells and connections between epigenetic methylations and the methyl metabolism of the cell have not been much considered.

Recently, it has emerged that epigenetic methylations are influenced by methyl donor nutrient availability, cellular levels of *S*-adenosylmethionine (SAM) and *S*-adenosylhomocysteine,[5,6] and competition with cytoplasmic methyltransferases including

Received: September 27, 2021
Published: February 23, 2022

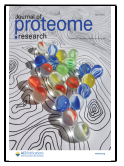

https://doi.org/10.1021/acs.jproteome.1c00778
J. Proteome Res. 2022, 21, 940−952

nicotinamide *N*-methyltransferase (NNMT),[7] glycine *N*-methyltransferase (GNMT),[8] and phosphatidylethanolamine *N*-methyltransferase (PEMT).[9]

SAM, the activated form of methionine, is the universal methyl group donor of the cell. SAM-dependent methyltransferases are numerous and methylate a wide range of targets from small molecules to proteins and nucleic acids. Not all targets are identified. Most expressed cytoplasmic methyltransferases include PEMT that methylates phosphatidylethanolamine to phosphatiylcholine (PtC), guanidinoacetate methyltransferase (GAMT) that methylates guanidinoacetate to creatine (Cr), and GNMT that methylates glycine (Gly) to sarcosine.[10] Little is known about their expression in tumor cells, although their activity is well known in body organs such as the liver.

Epigenetic methylations are dependent on SAM-dependent DNA and histone methyltransferases. Long believed to be static because of the covalent attachment of methyl residues to the acceptor, they are now recognized to be dynamic under the action of not only DNA and histone methyltransferases but also DNA and histone demethylases. Gene transcription thus depends on the methylation status of DNA and histones.

The methylation of cellular components may be probed by radiolabeled SAM or stable isotope-labeled methionine, or occasionally other labeled one-carbon sources. Stable isotope studies are not numerous. To investigate DNA or histone methylations, they made use of mass spectrometry with deuterium labeling of methyl groups[11−13] or NMR spectroscopy with ^{13}C labeling of methyl groups or one-carbon units.[14,15]

Specific epigenetic methylation marks are achievable by the aforementioned techniques. However, it would be of interest to have a comprehensive view of the interplay between methylases and between methylases and demethylases at the whole-cell scale. To this aim, untargeted metabolomics of tumor models labeled with a methyl-donor precursor, as achievable by NMR, is a tool validated by similar approaches with other precursors.[16]

Here, mouse tumor models were labeled with L-[^{13}C-*methyl*]methionine to search for their NMR-visible set of methyl acceptors, denoted the global methylome. Tumor models were B16 melanoma cell cultures and B16 melanoma tumors, which may be considered as two stages of B16 tumor development. We made use of 2D $^{1}H-^{13}C$ NMR spectroscopy sequences which are little applied in metabolomics, although they are recognized as pertinent in the field. We and others have proposed methods for exploiting 2D homonuclear or heteronuclear NMR signals in metabolomics.[17,18] In this study, data analysis was performed by orthogonal partial least squares discriminant analysis (OPLS-DA) of full-resolution 2D NMR spectra.

OPLS-DA revealed markedly different global methylomes for B16 melanoma cell cultures and B16 melanoma tumors. The methylome of B16 melanoma cell cultures was dominated by histone methylations and that of B16 melanoma tumors by cytoplasmic small-molecule methylations. Overall, OPLS-DA parameters mapped the non-DNA methylome. Comparison of the two tumor models exhibiting differential expression of aerobic glycolysis provided clues to a methyl metabolism shift during tumor progression.

METHODS

Chemicals

L-[^{13}C-*methyl*]Methionine ([^{13}C-*methyl*]Met) was obtained from Eurisotop (Gif-sur-Yvette, France). Unlabeled L-methionine (Met) was obtained from Sigma (St. Louis, MO) and deuterated water (D_2O) from SDS (Peypin, France).

B16 Melanoma Cell Cultures

Transplantable B16 (F1) melanoma cells originating from C57BL6/6J Ico mice were obtained from ICIG (Villejuif, France). Cells were maintained as monolayers in 75 cm^2 culture flasks in RPMI medium containing 100 μM Met (Sigma, St. Louis, MO) completed with 10% dialyzed fetal calf serum, 4 $\mu g \cdot mL^{-1}$ gentamicin, 50 $mg \cdot L^{-1}$ folic acid, and 1 $mg \cdot L^{-1}$ hydroxycobalamin. Melanocytes were maintained in 5% CO_2 and 90% humidity at 37 °C for 3−10 days. Cells were harvested by trypsinization, washed in PBS, centrifuged, and stored at −80 °C until exploitation.

Unlabeled B16 melanoma cell cultures were prepared as before. Labeled B16 melanoma cell cultures were prepared using a RPMI medium free of Met (Sigma) and supplemented with 100 μM labeled [^{13}C-*methyl*]Met. The medium was renewed every 2 days. After trypsinization, cells were washed in PBS and D_2O, centrifuged, and stored at −80 °C.

B16 Melanoma Tumors

Six- to eight-week-old C57BL6/6J male mice were inoculated with 5×10^5 B16 melanoma cells in one flank. Mice were housed by 3's in a polypropylene cage, in standard conditions of temperature and humidity, with an alternating 12 h light/dark cycle. All animal work was conducted in accordance with guidelines of the Animal Experimental Ethical Committee from Inserm. Animals were fed ad libitum a Met-deprived chow (INRAE, Jouy-en-Josas, France) and supplemented, in agreement with nutritional requirements, with 6 mg of Met, either unlabeled Met or [^{13}C-*methyl*]Met, twice daily, intraperitoneally. Mice were followed for body weight, physical appearance, behavior, and tumor size. They were sacrificed according to Institutional Guidelines for Animal's Welfare 15−25 days after B16 melanoma cell inoculation. Tumors were removed and weighed, and 20−40 μg intact samples were stored at −80 °C.

NMR Spectroscopy

NMR spectroscopy was performed on a small-bore 500 MHz Bruker Avance spectrometer (Bruker Biospin, Rheinstetten, Germany), equipped with a high-resolution magic angle spinning (HRMAS) probe. Intact cell pellets or tumor samples were set into 4-mm-diameter, 50-μL zirconium oxide rotor tubes with 2 drops of D_2O to lock the spectrometer. Rotors were spun at 4 kHz and cooled at 4 °C using the BCU-05 temperature unit.

A two-dimensional $^{1}H-^{13}C$ heteronuclear single quantum coherence (HSQC) sequence was used. Data were acquired with 5.48 ppm (^{1}H) × 120 ppm (^{13}C) spectral width, 1024 × 256 points, corresponding to a digital resolution of 2.7 Hz/point and 59 Hz/point along the direct and indirect dimensions (^{1}H and ^{13}C), respectively. The sequence used a 1.5-s relaxation delay, 64 transients, selection of coherences using phase cycling, and ^{13}C-decoupling during acquisition.

2D NMR Spectrum Processing

Minimal spectrum processing was performed using the Topspin Version 2.1 software (Bruker Biospin). 2D $^{1}H-^{13}C$ NMR spectra were reconstructed at a resolution of 1024 × 256. Mild apodization was performed. A 2D baseline correction was applied using a second-order polynomial.

Next, 2D NMR spectra were transferred to the Excel software (Microsoft). Spectra were calibrated on the easily identifiable signal of the methyl group of creatine (Cr CH_3), resonating at 3.035×38 ppm (all 2D NMR chemical shifts presented as

https://doi.org/10.1021/acs.jproteome.1c00778
J. Proteome Res. 2022, 21, 940−952

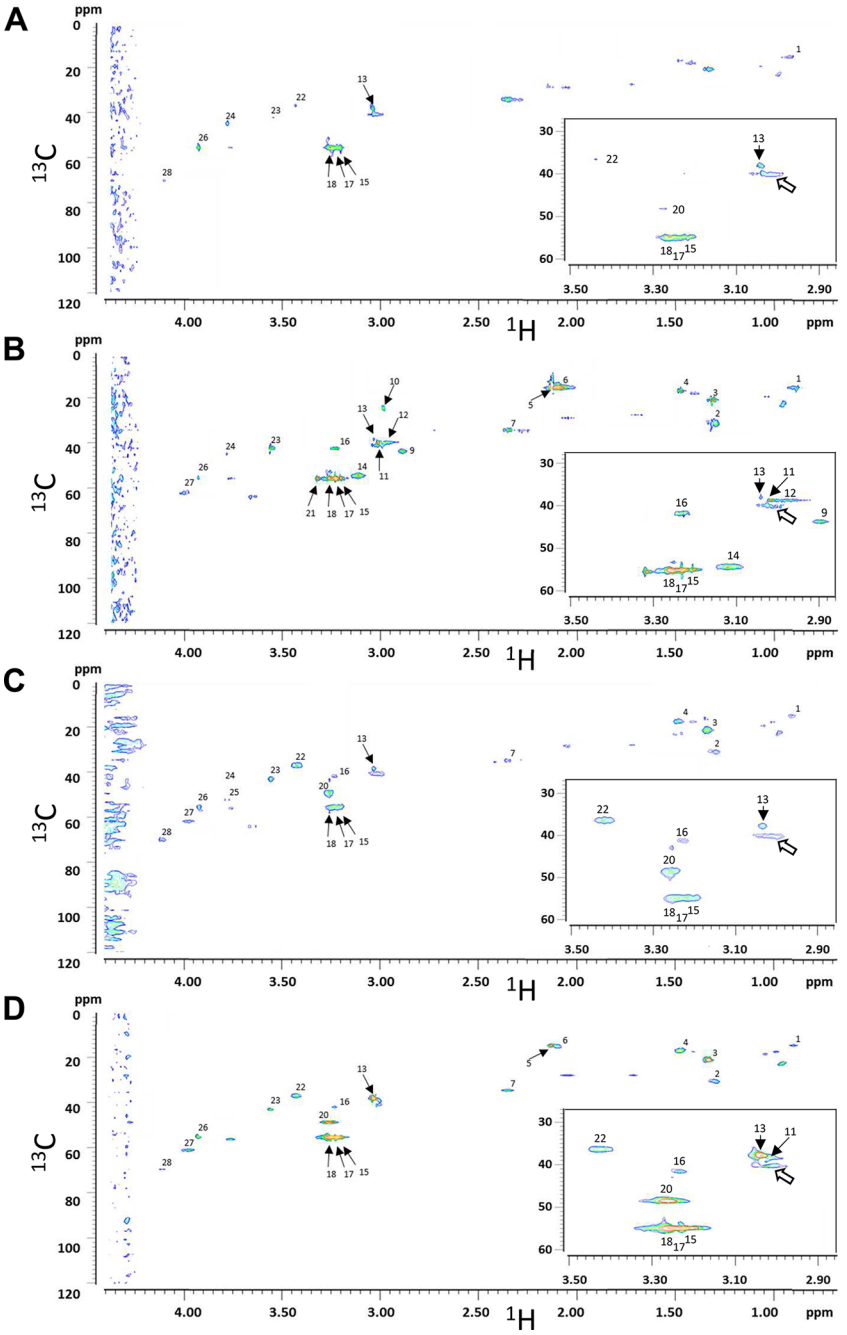

Figure 1. Typical HSQC spectra of intact B16 melanoma cell cultures and tumors in the (0.7−4.4 ppm)×(0−120 ppm) (^{1}H×^{13}C) spectral range. Unlabeled melanoma cell culture (A), [^{13}C-*methyl*]Met-labeled B16 melanoma cell culture (B), unlabeled melanoma tumor (C), and [^{13}C-*methyl*]Met-labeled melanoma tumor (D). Insets: (2.86−3.50 ppm)×(28−60 ppm) spectrum area. Cross-peaks of interest are numbered 1−28 (see Table 1). Open arrow: protein Lys CH_2-ε cross-peak.

^{1}H×^{13}C). The right wing of the residual water signal was removed to the left of 4.4 ppm. The final span of the spectrum was 0.7−4.4 ppm, corresponding to 692 data points along the ^{1}H-direction, and 0−120 ppm, corresponding to 256 data points along the ^{13}C-direction.

The easily identifiable signal of the ε-methylene of lysine (Lys CH_2-ε) bound to proteins, a broad cross-peak centered at 3.00×40 ppm, was observed in all spectra (labeled or not) due to the flexibility of the Lys side chain within proteins. Each spectrum was normalized to the cross-peak volume (CPV) of the protein Lys CH_2-ε cross-peak according to a quantitative NMR procedure that we previously developed.[17] The 2D NMR spectra were then linearized as column vectors of 177 152 (692 × 256, ^{1}H × ^{13}C) data points and were transferred to the OPLS-DA data processing software.

OPLS-DA of Full-Resolution 2D NMR Spectra

Spectra were imported into the SIMCA 14 software (Umetrics, Uppsala, Sweden) for OPLS-DA data processing. OPLS-DA is a metabolomics tool employed to generate a model of variable differences between two sets of annotated biological samples. Here variables were spectrum data points, and spectra were organized into two classes, depending on whether samples were labeled or not. After being normalized to the protein Lys CH_2-ε cross-peak, spectra were scaled in the centered mode.

https://doi.org/10.1021/acs.jproteome.1c00778
J. Proteome Res. 2022, 21, 940−952

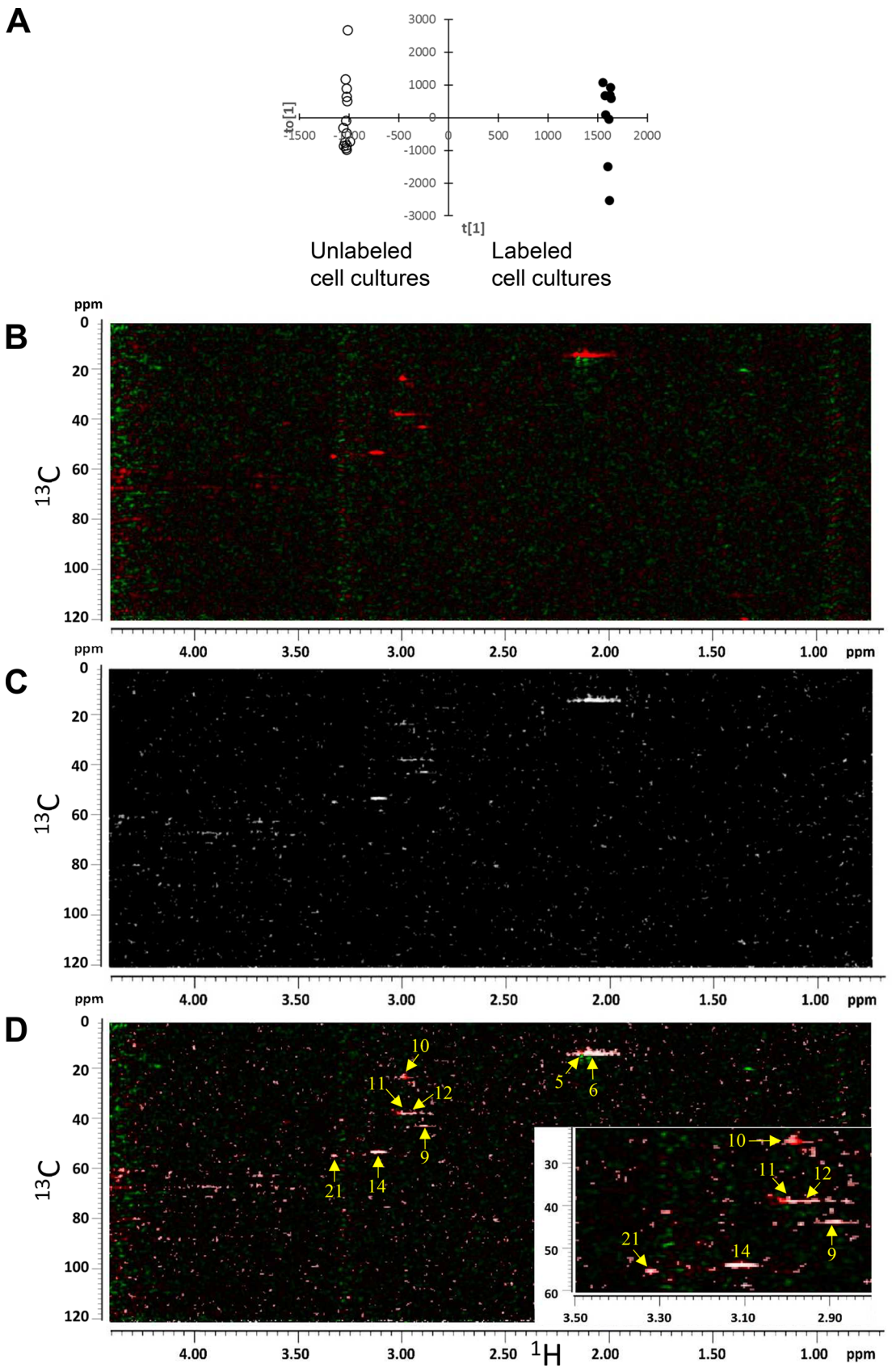

Figure 2. OPLS-DA of full-resolution 2D NMR spectra of unlabeled vs [^{13}C-*methyl*]Met-labeled B16 melanoma cell cultures. (A) Scores plot (to[1] vs t[1]) showing unlabeled (open circles) and labeled (full circles) cell cultures. (B) Loading plot of the predictive component (p(Ctr)[1]) displayed in the form of a 2D spectrum with the (0.7−4.4 ppm)×(0−120 ppm) (^{1}H×^{13}C) chemical shift range. (C) Correlation plot (p(corr)[1]) displayed in the form of a 2D NMR spectrum with a threshold of +0.50. (D) Merging of the previous two plots allowing to identify cross-peaks with both high loading

https://doi.org/10.1021/acs.jproteome.1c00778
J. Proteome Res. 2022, 21, 940−952

Figure 2. continued

and high correlation. Inset: (2.86−3.50 ppm)×(28−60 ppm) chemical shift area. Cross-peaks with both high p(Ctr)[1] and high p(corr)[1] are numbered (see Table 1).

Table 1. 2D Spectrum Cross-Peaks of Interest

	metabolite			cross-peak		chemical shifts	
no.	full name	abbreviation	group	abbreviation	structure[a]	^{1}H (ppm)	^{13}C (ppm)
1	fatty acids	FA	CH_3	FACH3		0.90	15
2	fatty acids	FA	$(CH_2)_n$	FACH2*n*		1.30	31
3	lactate	Lac	CH_3	LacCH3	thin	1.33	20
4	alanine	Ala	CH_3	AlaCH3	thin	1.47	17
5	methionine (free)	Met(f)	CH_3-S	Met(f)	thin	2.14	15
6	methionine (bound)	Met	CH_3-S	Met	broad	∼2.04−2.14	15
7	glutamate	Glu	γCH_2	GluCH2	thin	2.35	34
8	polyunsaturated fatty acids	PUF	CH═CH	PUF		2.82	26
9	dimethyllysine	$LysMe_2$	NMe_2	LysMe2	broad	∼2.87−2.89	44
10	*S*-adenosyl-methionine	SAM	CH_3-S	SAM	thin	2.98	24
11	a-dimethylarginine[b] (free)	$ArgMe_2$(f)	NMe_2	ArgMe2(f)	thin	3.01	39
12	a-dimethylarginine[b] (bound)	$ArgMe_2$	NMe_2	ArgMe2	broad	∼2.94−3.00	39
13	creatine	Cr	CH_3	CrCH3	thin	3.035	38
14	trimethyllysine	$LysMe_3$	NMe_3	LysMe3	broad	∼3.08−3.13	54
15	choline	Cho	NMe_3	Cho	thin	3.20	55
16	phosphoethanolamine	PE	CH_2-N	PECH2N	thin	3.22	41
17	phosphocholine	PC	NMe_3	PC	thin	3.22	55
18	phosphatidylcholine	PtC	NMe_3	PtC		3.26	55
19	glycine betaine	$GlyMe_3$	NMe_3	GlyMe3	thin	3.26	55
20	taurine	Tau	CH_2-S	TauCH2S	thin	3.27	48
21	unknown (assigned to serine betaine)			3.32×55 ppm	thin	3.32	55
22	taurine	Tau	CH_2-N	TauCH2N	thin	3.44	36
23	glycine	Gly	CH_2	Gly	thin	3.56	42
24	glutathione	GSH	CH_2 (Gly)	GSH	thin	3.78	44
25	alanine	Ala	CH	AlaCH	thin	3.78	52
26	creatine	Cr	CH_2	CrCH2	thin	3.93	55
27	phosphoethanolamine	PE	CH_2-O	PECH2O	thin	3.99	62
28	lactate	Lac	CH	LacCH	thin	4.11	69

[a]A cross-peak with a thin structure may be a multiplet. [b]Asymmetric dimethylarginine.

OPLS-DA operates as follows. First, data that is orthogonal (uncorrelated) to the classes is removed from the analysis. Second, the remaining data is processed by partial least squares discriminant analysis, yielding a predictive component which models the differences between labeled and unlabeled spectra. Finally, orthogonal components are calculated, each one bringing some improvement to the predictive component. However, to prevent overfitting of data, a cross-validation process is applied to decide whether a component is significant or not.

The overall quality of the model is summarized by R2X, R2Y, Q2, and the p-value of CV-ANOVA that designate the percentage of explained variance of data (total variance = 1), the explained variance of classes, the cross-validated variance of data, and the cross-validated ANOVA. For the latter, a p-value below 0.05 indicated a statistically significant model. R2X and Q2 parameters for a good model are close to 0.5 or higher.

OPLS-DA provided the following parameters: (i) t[1] and to[1] scores, the projection of individual samples on the predictive and first orthogonal components, (ii) p(Ctr)[1] loadings, the contribution of variables (spectrum data points) to the predictive component, and (iii) p(corr)[1], the correlation coefficients associated with loadings.

A plot of p(corr)[1] correlation coefficients against p(Ctr)[1] loadings, denoted an S-plot, is the usual way to identify variables at the extremities of the S-plot that strongly contribute to the model. These variables are markers of the difference between the two groups. In this study, markers were spectrum data points that strongly correlated with labeling, thus were ^{13}C-labeled. Labeled signals cannot exhibit negative p(Ctr)[1] or p(corr)[1] values since ^{13}C-labeling univocally increases the signal.

For exploitation of OPLS-DA results, p(Ctr)[1] and p(corr)-[1] were transferred to the Excel software and reconstructed similarly as 2D NMR spectra with a 692 × 256 resolution. A mild adaptation of the S-plot strategy to the 2D display was to superpose the p(Ctr)[1] and p(corr)[1] maps to highlight signals with both high p(Ctr)[1] and high p(corr)[1]. We chose to display the p(Ctr)[1] map with a green-red color scale and the p(corr)[1] map with a gray scale. For the latter, since labeled cross-peaks cannot be negative, and since spectral noise causes many spurious correlations, a mild smoothing and a statistical cutoff improved the display.

Therefore, p(Ctr)[1], p(corr)[1], and merging maps summarized the full set of 2D ^{1}H−^{13}C NMR spectra and were used to identify labeled cross-peaks. Chemical shifts of labeled cross-peaks were obtained from the literature.

https://doi.org/10.1021/acs.jproteome.1c00778
J. Proteome Res. 2022, 21, 940−952

Measurements within full-resolution $p(\mathrm{Ctr})[1]$ and $p(\mathrm{corr})[1]$ maps were limited to regions of interest (ROIs) delineated over cross-peaks of interest. For labeled cross-peaks, the delineation of ROIs was facilitated by $p(\mathrm{Ctr})[1]$, $p(\mathrm{corr})[1]$, and merging maps. For unlabeled cross-peaks, ROI delineation was based on sufficient signal-to-noise ratios in raw spectra. Twenty-eight ROIs were drawn. An Excel script made it possible to compute various parameters within these ROIs. The parameters calculated in ROIs included the largest value of $p(\mathrm{Ctr})[1]$, the average value of $p(\mathrm{Ctr})[1]$, the largest value of $p(\mathrm{corr})[1]$, and the number of pixels with $p(\mathrm{corr})[1]$ higher than 0.5. These parameters were ranked over the set of ROIs, and then ranks were summed to compute a final score. This score further quantified the information on $p(\mathrm{Ctr})[1]$ and $p(\mathrm{corr})[1]$ and provided a ranking of cross-peaks for labeling.

OPLS-DA of 2D NMR Spectrum ROIs

We used the same ROIs as before. CPVs were calculated in ROIs using an Excel script for each 2D $^{1}H-^{13}C$ NMR raw spectrum. OPLS-DA was performed on CPVs. Data processing was the same as that for full-resolution spectra. Due to the dramatic reduction of variables, interpretation was based on the classical S-plot display of $p(\mathrm{corr})[1]$ against $p(\mathrm{Ctr})[1]$. Results were compared to those of OPLS-DA of full-resolution 2D NMR spectra.

^{13}C Fractional Enrichment

The ^{13}C fractional enrichment of a metabolite group (^{13}C incorporation above natural abundance) was calculated using the corresponding CPV as $[\mathrm{CPV(labeled\ individual)/mean\ CPV(unlabeled\ individuals)} - 1] \times 1.1\%$, where 1.1% represents the ^{13}C natural abundance. Comparison of means was performed using the bilateral Student t test and considered significant for p-values below 0.05.

RESULTS

B16 Melanoma Cell Methylome Is Dominated by Epigenetic Methylations

Typical 2D $^{1}H-^{13}C$ HSQC spectra of unlabeled and labeled B16 melanoma cell cultures are displayed in Figure 1A,B. The number of samples was $n = 9$ for unlabeled cell cultures and $n = 14$ for labeled cell cultures.

The OPLS-DA model of full-resolution 2D NMR spectra was obtained with one predictive and seven significant orthogonal components, R2 and Q2 parameters of 0.569 and 0.844, respectively, and a cross-validated ANOVA test at $p = 0.012$ (Figure 2). Scores of individual spectra were plotted along the predictive axis and the first orthogonal component (Figure 2A). They showed excellent separation of labeled vs unlabeled samples by the model.

Superposition of parameter maps (Figure 2D) showed cross-peaks with both high $p(\mathrm{Ctr})[1]$ and high $p(\mathrm{corr})[1]$ that highly contributed to the difference between labeled and unlabeled spectra, including LysMe3, LysMe2, ArgMe2, ArgMe2(f), Met, and Met(f) (Table 1). Only asymmetric dimethylarginine ($ArgMe_2$), not symmetric (cross-peak at ~2.75×26 ppm), was highlighted as labeled. As well, monomethylarginine was not observed. In association with Met and ArgMe2 broad cross-peaks, we observed thin cross-peaks corresponding to the same molecule in the free state, denoted Met(f) and ArgMe2(f). As shown in the Discussion, for quantitative and qualitative reasons, $LysMe_3$, $LysMe_2$, and $ArgMe_2$ labeled signals originated from histones. In contrast, no 5-methylcytosine labeling (cross-peak at ~1.7×14 ppm[15]) originating from DNA was observed. Putative cytosolic methyl acceptors such as PtC and Cr were not labeled (signals at 3.26×55 and 3.035×38 ppm, respectively).

Then, scores for labeling were calculated in the set of ROIs drawn on full-resolution $p(\mathrm{Ctr})[1]$ and $p(\mathrm{corr})[1]$ maps. Calculated scores of cross-peaks are displayed in Figure 3A

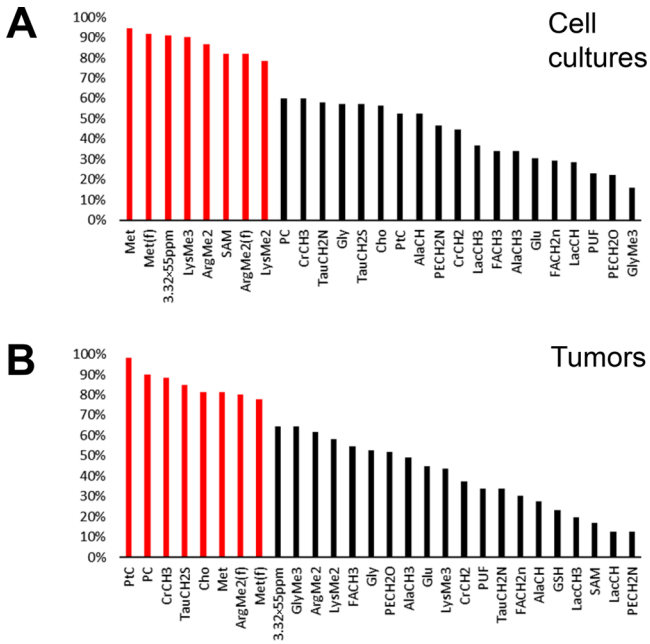

Figure 3. Scores for labeling likelihood calculated from OPLS-DA results of full-resolution spectra over the series of 28 spectrum cross-peaks. (A) B16 melanoma cell cultures and (B) B16 melanoma tumors. Red bars indicate the highest values to the left of a step in the ranked scores.

showing a step in the ranked scores to the left of which we retained cross-peaks with the highest probability to be labeled. These cross-peaks were, in decreasing order Met, Met(f), 3.32×55 ppm, LysMe3, ArgMe2, SAM, ArgMe2(f), and LysMe2.

Further, we measured CPVs in ROIs drawn on raw 2D NMR spectra and applied OPLS-DA to these data (OPLS-DA of spectrum ROIs). Quality parameters of OPLS-DA were R2 = 0.491, Q2 = 0.531, and $p = 0.006$. The model was obtained with the predictive and one significant orthogonal component. The comparison between unlabeled and labeled B16 melanoma cells is given in Figure 4A,B. The S-plot revealed that labeled cross-peaks, combining high $p(\mathrm{Ctr})[1]$ and high $p(\mathrm{corr})[1]$, were Met(f), ArgMe2(f), Met, 3.32×55 ppm, LysMe3, ArgMe2, and LysMe2. According to the S-plot, SAM and GlyMe3, with $p(\mathrm{corr})[1] \approx +0.40$, had lower probability to be labeled. The ^{13}C fractional enrichment of metabolite groups identified as labeled in tumors is given in Table 2.

OPLS-DA of both full-resolution spectra (Figure 2) and spectrum ROIs (Figure 4A,B) highlighted a labeled signal at 3.32×55 ppm. We did not find assignment for this signal in NMR literature and metabolomics databases. Unfortunately, NMR annotation software (NMRshiftDB, ChemDraw) did not provide sufficient ^{1}H chemical shift accuracy for proper assignment. We thus sought for a candidate metabolite based on biological considerations and analogy with literature-available assignments.

https://doi.org/10.1021/acs.jproteome.1c00778
J. Proteome Res. 2022, 21, 940−952

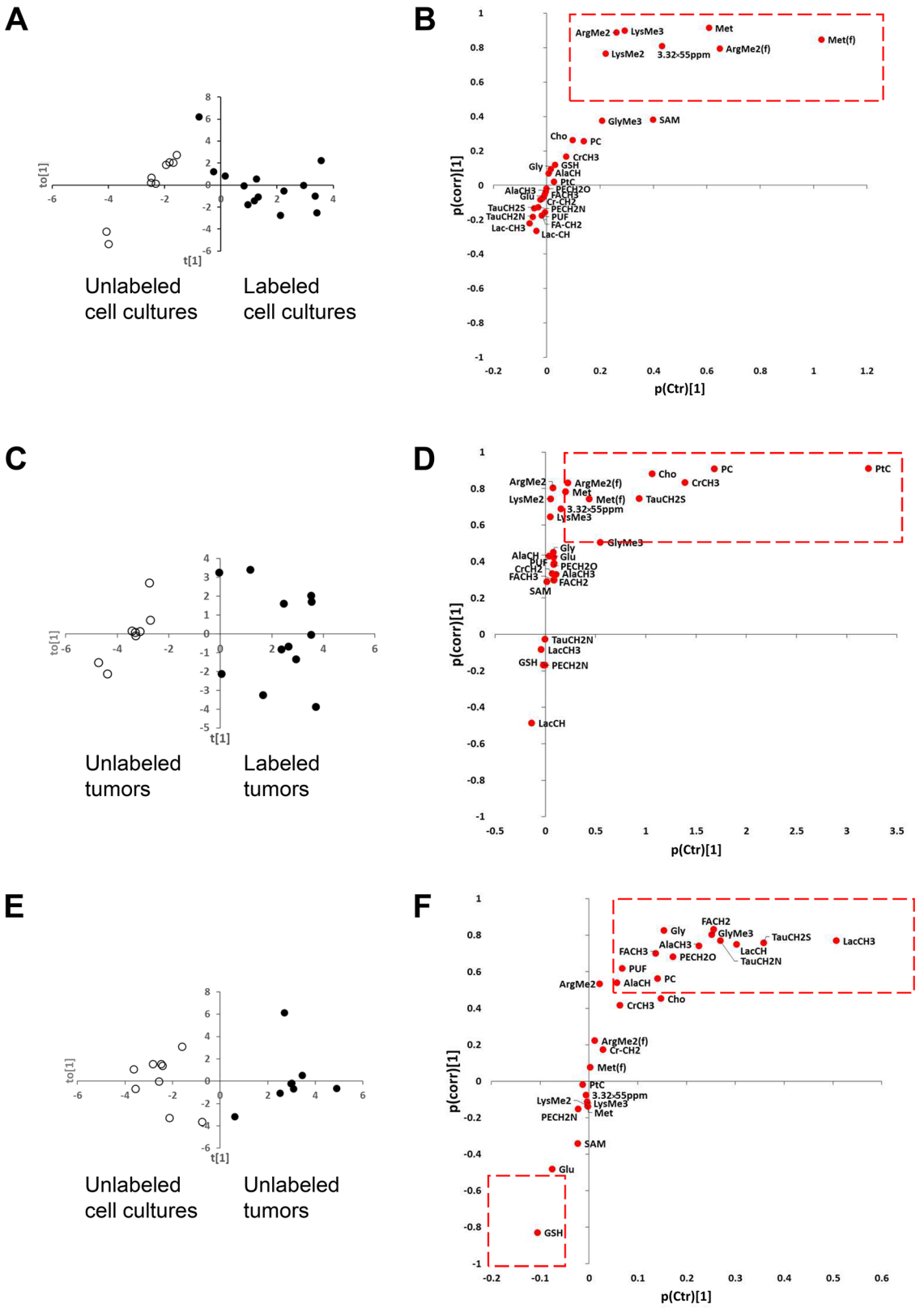

Figure 4. OPLS-DA of 2D NMR spectrum ROIs (n = 28). (A, B) Scores plot (A) of unlabeled (open circles) vs [^{13}C-*methyl*]Met-labeled (full circles) B16 melanoma cell cultures and S-plot (B). (C, D) Scores plot (C) of unlabeled (open circles) vs [^{13}C-*methyl*]Met-labeled (full circles) B16 melanoma tumors and S-plot (D). (E, F) Scores plot (E) of unlabeled B16 melanoma cell cultures (open circles) vs unlabeled B16 melanoma tumors (full circles) and S-plot (F). The dotted rectangles indicate the S-plot area containing cross-peaks with both high p(Ctr)[1] and high p(corr)[1] (here, absolute value between 0.50 and 1).

First, we eliminated methyl residues of aliphatic or aromatic backbones, methyl-sulfonium derivatives, methoxy derivatives, and O-methyl esters. None of these signals fell within the right chemical shift area. We ruled out tetramethylammonium

https://doi.org/10.1021/acs.jproteome.1c00778
J. Proteome Res. 2022, 21, 940−952

Table 2. ^{13}C Fractional Enrichment of Labeled Metabolite Groups in B16 Melanoma Cell Cultures

	unlabeled, n = 9		labeled, n = 14		
cross-peak[a]	mean (%)	SD (%)	mean (%)	SD (%)	p-value
Met	0.0	0.7	32.2	13.6	0.0000
Met(f)	0.0	0.8	34.6	22.3	0.0001
3.32×55 ppm	0.0	0.9	13.0	9.0	0.0001
LysMe3	0.0	1.2	11.7	9.4	0.0004
ArgMe2	0.0	3.3	n.c.[b]	n.c.	–
SAM	0.0	1.0	9.4	9.1	0.0028
ArgMe2(f)	0.0	2.8	n.c.	n.c.	–
LysMe2	0.0	1.1	14.8	10.5	0.0002

[a]Cross-peak abbreviation, see Table 1. [b]n.c. = not calculated.

reported at 3.18×58 ppm.[19] It remained trimethylammonium (NMe_3^+) residues that lie in the (3.05−3.40 ppm)×(46−58 ppm) spectrum area.[20] Among them, those with a ^1H chemical shift above 3.26 ppm, were amino acid betaines. The best known of them is glycine betaine resonating at 3.26×55 ppm. Indeed, in the literature reported in Table 3, we found amino acid betaines with ^1H chemical shifts above 3.26 ppm, namely histidine betaine (3.27 ppm),[21] threonine betaine (3.29 ppm),[22] ergothioneine (3.28 ppm),[23,24] and proline betaine, all reported with a 55 ± 1 ppm ^{13}C chemical shift.

To get closer to the target ^1H chemical shift, we sought to determine the effect of hydroxylation at the beta-position. From Table 3, this modification should cause a ^1H chemical shift increase of about 0.11 ppm. Starting from alanine betaine, β-hydroxylation should yield serine betaine and move the chemical shift from about 3.20 ppm to about 3.31 ppm. Similar reasoning may be performed with other molecule residues. We found in the literature serine betaine ethers with a chemical shift in methanol from 3.32 to 3.38 ppm.[25] Overall our most likely assignment for the 3.32×55 ppm cross-peak was *N,N,N*-trimethylserine or serine betaine, a methylated species that joined the methylome of B16 melanoma cells. We did not attempt to synthesize the molecule to confirm the chemical shift with our technique since there is no doubt that the guessed NMe_3^+ signal will match but would leave serine betaine as a very likely hypothesis.

B16 Melanoma Tumor Methylome Is Dominated by Cytoplasmic Small-Molecule Methylations

Typical 2D $^1H-^{13}C$ HSQC spectra of unlabeled and labeled B16 melanoma tumors are displayed in Figure 1C,D. The number of samples was n = 8 for unlabeled tumors and n = 12 for labeled tumors.

The OPLS-DA model of full-resolution 2D NMR spectra was obtained with one predictive and six significant orthogonal components, R2 and Q2 parameters of 0.537 and 0.838, respectively, and a cross-validated ANOVA test at p = 0.015 (Figure 5). Scores of individual spectra were plotted along the predictive axis and the first orthogonal component (Figure 5A). It showed excellent separation of labeled vs unlabeled samples by the model.

Superposition of parameter maps (Figure 5D) showed cross-peaks with both high p(Ctr)[1] and high p(corr)[1] that

Table 3. Literature Used for the Assignment of the 3.32×55 ppm (^1H×^{13}C) Cross-Peak

amino acid betaine	betaine position[a]	solvent	internal standard[b]	$\delta(^1H)$ (ppm)	$\delta(^{13}C)$ (ppm)	ref	β-hydroxylated form	solvent	internal standard	$\delta(^1H)$ (ppm)	$\delta(^{13}C)$ (ppm)	ref
α-amino-butyric acid-betaine	α	D_2O	TSP	3.20		36	threonine-betaine	D_2O	DSS	3.29		22
γ-amino-butyric acid-betaine	γ	D_2O	TFA	3.05		37	carnitine	D_2O	TFA	3.15		37
		D_2O	DSS	3.12		20		D_2O	DSS	3.22		20
		D_2O	DSS	3.12		21		D_2O	DSS	3.22	57	38
lysine-betaine	ε	D_2O	TSP	3.12		39						
		D_2O	–	3.06	53	40						
		D_2O	DSS	3.11		21						
		D_2O	DSS	3.04	53	41						
	α	D_2O	–	3.17	53	40						
		D_2O	DSS	3.12	52	41						
alanine-betaine	α	D_2O	DSS	3.18	55	20	serine-betaine					
		D_2O	TSP	3.23		42	1,2-dipropionyl-glyceryl-3-*O*-3′-serine-betaine	CD_3OD	TMS	3.32	54	25
		D_2O	DSS	3.20	53	22						
glycine-betaine	α	D_2O	DSS	3.26	56	20						
		D_2O	DSS	3.26		21						
		D_2O	TSP	3.27	56	43						
histidine-betaine	α	D_2O	DSS	3.26		21						
		D_2O	DSS	3.27	55	20						
ergothioneine	α	D_2O	DSS	3.28	55	23	β-hydroxy-ergothioneine	D_2O	DSS	3.39	56	23
		D_2O	TSP	3.27		24						

[a]Position from the carboxylic group. [b]Abbreviations: TSP, sodium 3-trimethylsilyl(2,2,3,3-$^2H_4$)propionate; DSS, sodium 2,2-dimethyl-2-silapentane-5-sulfonate-$^2H_6$; TFA, 1,1,1-trifluoroacetone; TMS, tetramethylsilane.

https://doi.org/10.1021/acs.jproteome.1c00778
J. Proteome Res. 2022, 21, 940−952

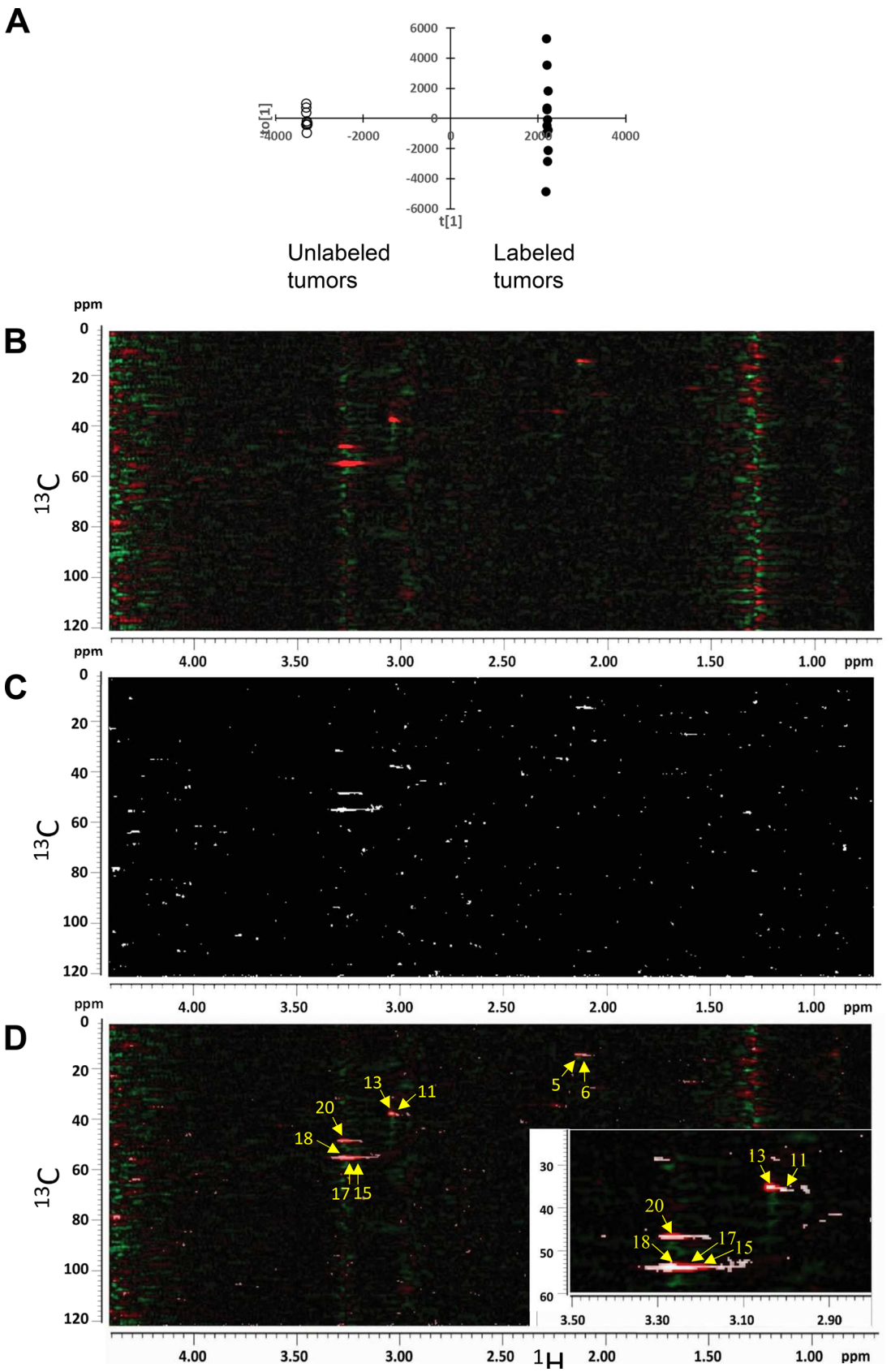

Figure 5. OPLS-DA of full-resolution 2D NMR spectra of unlabeled vs [^{13}C-*methyl*]Met-labeled B16 melanoma tumors. (A) Scores plot showing unlabeled (open circles) and labeled (full circles) tumors. (B) Loading plot of the predictive component (p(Ctr)[1]) displayed in the form of a 2D NMR spectrum with the (0.7−4.4 ppm)×(0−120 ppm) chemical shift range. (C) Correlation plot (p(corr)[1]) displayed in the form of a 2D NMR spectrum with a threshold of +0.50. (D) merging of the previous two plots, allowing to identify cross-peaks with both high loading and high correlation. Inset: (2.86−3.50 ppm)×(28−60 ppm) chemical shift area. Cross-peaks with both high p(Ctr)[1] and high p(corr)[1] are numbered (see Table 1).

https://doi.org/10.1021/acs.jproteome.1c00778
J. Proteome Res. 2022, 21, 940−952

contributed highly to the difference between labeled and unlabeled spectra, including PtC, PC, Cho, CrCH3, Met, and ArgMe2(f) and, unexpectedly, TauCH2S. This cross-peak corresponded to the C_1-carbon of Tau, besides the sulfur atom.[26,27] Tau is one of the end-course products of transsulfuration. This prompted us to verify that neither GSH nor pyruvate, two other products of transsulfuration, gave rise to labeled signals. Only noise was observed at the expected spectral positions (2.36×29 and 2.96×28 ppm, respectively). Nevertheless, in 2 of our 12 labeled tumor spectra, we found a quite intense cysteine CH_2 cross-peak (corresponding to the C_3-carbon) around 3.08×26 ppm (Figure S1), but this cross-peak did not appear in p(Ctr)[1] or p(corr)[1] maps. No signal from the transmethylation product, sarcosine, (2.72×36 ppm) was observed.

Then scores for labeling were calculated in the set of ROIs drawn on full-resolution p(Ctr)[1] and p(corr)[1] maps. Calculated scores of cross-peaks are displayed in Figure 3B, showing a step in the ranked scores to the left of which we retained cross-peaks with the highest probability to be labeled. These cross-peaks were, in decreasing order, PtC, PC, CrCH3, TauCH2S, Cho, Met, ArgMe2(f), and Met(f).

Further, we measured CPVs in ROIs drawn on raw 2D NMR spectra and applied OPLS-DA to these data (OPLS-DA of spectrum ROIs). Quality parameters of OPLS-DA were R2 = 0.590, Q2 = 0.755, and p = 0.0002. The model was obtained with the predictive and one significant orthogonal component. The comparison between unlabeled and labeled B16 melanoma tumors is given in Figure 4C,D. The S-plot revealed that labeled cross-peaks, combining high p(Ctr)[1] and high p(corr)[1], were PtC, PC, CrCH3, Cho, TauCH2S, Met(f), ArgMe2(f), and Met. According to the S-plot, GlyMe3 and 3.32×55 ppm had borderline probability to be labeled. However, their labeling was litigious since these cross-peaks lay in the vicinity of a strongly labeled one, PtC. The ^{13}C fractional enrichment of metabolite groups identified as labeled in tumors is given in Table 4.

Table 4. ^{13}C Fractional Enrichment of Labeled Metabolite Groups in B16 Melanoma Tumors

	unlabeled, n = 8		labeled, n = 12		
cross-peak[a]	mean (%)	SD (%)	mean (%)	SD (%)	p-value
PtC	0.0	0.4	3.7	2.4	0.0002
PC	0.0	0.3	3.3	1.3	0.0000
CrCH3	0.0	0.3	6.4	3.5	0.0001
TauCH2S	0.0	0.3	1.9	1.2	0.0002
Cho	0.0	0.6	2.9	1.3	0.0000
Met(f)	0.0	0.7	17.2	11.8	0.0004
ArgMe2(f)	0.0	1.7	11.9	7.9	0.0003
Met	0.0	0.7	14.7	9.2	0.0002

[a]Cross-peak abbreviation, see Table 1.

B16 Melanoma Cells and Tumors Differ for Bioenergetic Metabolism

To look at metabolic differences between unlabeled tumor models, we used CPVs measured in 2D NMR spectra of unlabeled melanoma cell cultures (n = 9) and melanoma tumors (n = 8). OPLS-DA was applied to these data (Figure 4E,F). Quality parameters of OPLS-DA were R2 = 0.591, Q2 = 0.715, and p = 0.004. The model was obtained with the predictive and one significant orthogonal component. The classical S-plot of p(corr)[1] against p(Ctr)[1] was used to interpret the results. Unlabeled melanoma cells expressed a high level of GSH, the major antioxidant of the cell that plays a role in detoxifying mitochondrially produced ROS, in favor of still active oxidative phosphorylation. In contrast, in unlabeled B16 tumors, the strongest signals revealed by the S-plot were LacCH3, TauCH2S, LacCH, TauCH2N, FACH2, GlyMe3, and AlaCH3. Lac was the major glycolysis byproduct, and the high levels of biosynthetic molecules like FA and non-essential amino acids (glycine (Gly), alanine (Ala), and taurine (Tau)) indicated that the B16 tumor's central metabolism relied on aerobic glycolysis. Overall, the canonical switch to aerobic glycolysis occurred between B16 melanoma cell cultures and B16 melanoma tumors, the two stages of our B16 tumor progression model.

DISCUSSION

Methodological Considerations

In this study, we sought to map metabolites downstream of Met having incorporated the Met methyl carbon. The study exploited 2D $^1H-^{13}C$ NMR spectra of tumor models labeled with [^{13}C-*methyl*]Met and metabolomics data processing using OPLS-DA of NMR spectra at full resolution. The Kegg pathway database[28] reports that metabolites that may incorporate the Met methyl carbon include, besides Met free and bound to macromolecules, (i) SAM, (ii) transmethylation products or methyl acceptors, and (iii) *S*-methyl-5-thioadenosine and derivatives of the Met salvage pathway. SAM is synthesized by the activity of methionine-adenosyltransferase. *S*-Methyl-5-thioadenosine is synthesized by the activity of enzymes of polyamine synthesis. Most methylated derivatives resonate at specific positions in $^1H-^{13}C$ NMR spectra as shown by NMR assignment databases. The best known SAM-dependent transmethylations are displayed in Figure 6A.

The method used gave access to the non-DNA methylome. No signal of the 5-methylation of cytosine residues within DNA CpG islands was found, probably due to reduced molecular flexibility.[15] In contrast, histone methylation at Lys and Arg residues is visible after labeling using NMR techniques. This is due to the high flexibility of histone tails, as reported for bacteria cultured in ^{13}C-labeled glucose.[29] Other conditions improving histone *N*-methylation visibility include the 2- or 3-fold methylation of residues and the several methylated residues of the tail that merge into the same broad signals. Note that monomethyllysine and monomethylarginine cross-peaks (~2.7×35.5 and ~2.8×26 ppm, respectively) were not found in our spectra. This observation may set a lower limit to histone methylation detection with our technique.

Non-histone proteins may be lysine-methylated, some of them being implicated in carcinogenesis, like p53. However, their content is lower than that of histones, few are trimethylated, methylations frequently occur at their C-termini, and their structure may not be as flexible as that of histone N-tails.

Few studies using stable isotopes aimed at demonstrating a relationship between one-carbon metabolism and histone methylation. HeLa cells labeled with L-[^2H,^2H,^2H,^{13}C-*methyl*]-Met incorporated the $^{13}C^2H_3$ methyl residue, as demonstrated by LCMS, at several histone lysine positions.[12] Using mass spectrometry of histones from leukemia cells exposed to [2,3,3-^2H]serine, it was shown that ^2H atoms were transferred from serine to *N*-methyl residues of $LysMe_3$.[11]

https://doi.org/10.1021/acs.jproteome.1c00778
J. Proteome Res. 2022, 21, 940−952

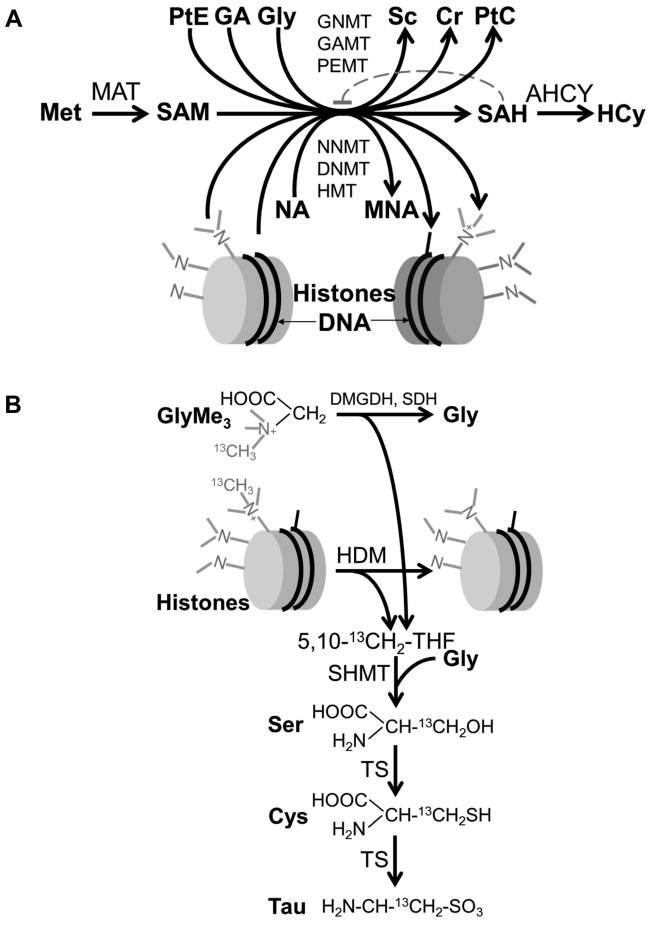

Figure 6. (A) SAM-dependent methyltranferases in mammalian cells. Displayed transmethylations are not exhaustive. Abbreviations: PtE, phosphatidylethanolamine; GA, guanidinoacetate; Sc, sarcosine; SAH, *S*-adenosylhomocysteine; HCy, homocysteine; NA, nicotinamide; MNA, 1-methylnicotinamide; MAT, methionine adenosyltransferase; DNMT, DNA methyltransferases; HMT, histone methyltransferases; AHCY, adenosylhomocysteinase. Other abbreviations, see text. SAH exerts an allosteric inhibition on methyltransferases (dashed line). (B) Biochemical hypotheses about how C_1-carbon labeling of Tau is related to the activity of known demethylases. Abbreviations: ^{13}C, labeled carbon; 5,10-CH_2-THF, 5,10-methylenetetrahydrofolate; Ser, serine; Cys, cysteine; DMGDH, dimethylglycine dehydrogenase; SDH, sarcosine dehydrogenase; HDM, histone demethylases; SHMT, serine hydroxymethyltransferase; TS, transsulfuration. Other abbreviations, see text.

In this study, unprecedentedly to our knowledge, p(Ctr)[1] and p(corr)[1] maps generated by OPLS-DA data processing of full-resolution 2D $^{1}H-^{13}C$ NMR spectra were obtained to automatically identify signals having incorporated the label from a ^{13}C-labeled precursor. With [^{13}C-*methyl*]Met labeling, p(Ctr)-[1] and p(corr)[1] maps highlighted the global methylome.

We faced a limitation in identifying labeled molecules with OPLS-DA. In a few tumor spectra, cysteine was very likely labeled at its C_3-position. Because of insufficient representation throughout samples, the signal did not appear in p(Ctr)[1] or p(corr)[1] maps.

Despite that, full-resolution spectrum OPLS-DA is an automatic procedure that may assist exploitation of 2D NMR spectra in future studies, as these spectra will become increasingly available due to improvements in fast 2D acquisitions and signal-to-noise ratio with cooled coils.

B16 Melanoma Cell Culture Methylome

The two major features of the methylome of B16 melanoma cells were (i) strong methylation of histone tails in the form of $ArgMe_2$, $LysMe_2$, and $LysMe_3$ residues and (ii) lack of incorporation of methionine-originating methyl groups into the main small-molecule acceptors, Cr and PtC.

We found that histone methylation including $ArgMe_2$, $LysMe_2$, and $LysMe_3$ residues was abundant. This raises the question as to whether histones in B16 melanoma cell cultures were globally hypermethylated. It was suggested that histones have the capacity to store substantial amounts of methyl groups for metabolic purposes, beyond a role in transcriptional regulation.[30] Other conditions yielding to global methylation of histones include hyperactivation of NNMT[7] and gain-of-function mutation of isocitrate dehydrogenase-1/2 (IDH1/2).[31] However, we could rule out these conditions since we found no significant signal of 1-methylnicotinamide (methyl residue at 4.49×49 ppm), 2-hydroxyglutarate,[32] or succinate (2.39×37 ppm). Another report showed that cells lacking PEMT activity exhibited global hypermethylation of histones.[9] This is agreement with our findings in B16 melanoma cells which do not exhibit labeling of the NMe_3^+ group of PtC, thus appear defective in PEMT activity.

Our best assignment for the 3.32×55 ppm signal was serine betaine, an *α-N,N,N*-trimethylated amino acid as $GlyMe_3$. Evidence of assignment would require a quite complex structural elucidation (dual labeling, triple-resonance NMR experiments, etc.), not simply the confrontation to an authentic standard. At present, little is known about serine betaine. It is reported as a post-translational modification of some proteins involved in chromatin structure.[33] This post-translational modification is not reported in mice yet.

B16 Melanoma Tumor Methylome

The two major features of the methylome of B16 tumors were (i) low methylation of Lys and Arg in histone tails and (ii) substantial incorporation of ^{13}C into small metabolites, namely Cr and PtC derivatives. Levels of $ArgMe_2$, $LysMe_2$, and $LysMe_3$ were lower in melanoma tumors vs melanoma cells, with $LysMe_3$ decreasing the most, in favor of decreased histone methylation or increased histone demethylation. We could verify in tumor spectra that we had no accumulating signal from 1-methylnicotinamide, 2-hydroxyglutarate, or succinate. In contrast to the B16 melanoma cell cultures, Cr and PtC were quite strongly labeled. Their origin may be activation of GAMT and PEMT in tumors. Unfortunately, little data is available about these metabolic pathways in tumors.

A finding in labeled tumors was that the Met methyl carbon was incorporated in a significant amount into the CH_2-S carbon of Tau, a transulfuration end-course product. It has been reported that overexpression of PEMT in tumor cells yielded increased transsulfuration activity,[9] which is consistent with our finding of joint labeling of Tau and PtC. The Tau CH_2-S carbon originates from the C_3-carbon of serine.[28] Serine is synthesized from Gly and 5,10-methylene-tetrahydrofolate (5,10-CH_2-THF) by serine hydroxymethyltransferase (Figure 6B). In the one-carbon cycle, 5,10-CH_2-THF is synthesized from THF and formaldehyde.

Finally, the question arises as to where formaldehyde comes from. Formaldehyde is a genotoxic byproduct that must be detoxified in mammals.[34] According to the literature, formaldehyde is a product of oxidative demethylation. Oxidative demethylation occurs in a limited number of reactions, namely

https://doi.org/10.1021/acs.jproteome.1c00778
J. Proteome Res. 2022, 21, 940−952

demethylation of dimethylglycine and sarcosine by dimethylglycine and sarcosine dehydrogenases[35] and demethylation of histones by histone demethylases[31] (Figure 6B). In the B16 melanoma tumor methylome, we found a moderate signal of $GlyMe_3$, the precursor of dimethylglycine and sarcosine, but no signals of dimethylglycine or sarcosine. This pathway of demethylation is known in the liver but little investigated in other tissues. It was reported to be expressed in prostate cancer.[35] Alternatively, histone methylation exhibited low levels in tumors, especially $LysMe_3$, that is expected to be targeted first by demethylases because of its role in gene expression regulation. This may indicate histone demethylation activation in B16 melanoma tumors.

Some fates of the methyl carbon of [^{13}C-*methyl*]Met are assignable to tumor metabolism, including incorporation into proteins and histone methylation. However, little knowledge is available on PEMT, GAMT, and oxidative demethylation pathways in tumors. So the question arises whether the observed metabolites (PtC, Cr, and Tau) could not be taken up from the blood, especially originating from the liver. The liver is known to produce a wealth of compounds, one of which is glucose, a nutrient for many organs and tumors. However, we found an unambiguous signal of cysteine CH_2 (C_3-carbon) in a few tumor spectra, the intensity of which indicated labeling. This finding supported Tau synthesis in the tumor, although it did not eliminate an uptake of cysteine further metabolized into Tau. Also, we did not find in tumors labeled metabolites that may trace a liver origin such as sarcosine. It is important to ensure the origin of labeled metabolites in tumors, not only to clarify the metabolome of tumors but also since this knowledge may be applied to target the tumor.

Methyl Group Metabolism during Tumor Progression

At baseline, the bioenergetic phenotype of B16 melanoma cells was dominated by oxidative phosphorylation, whereas that of melanoma tumors was dominated by aerobic glycolysis. Morphological changes between cells and tumors include 3D mass and microenvironment formation. Cells of the microenvironment play a role in nutritional exchanges with tumor cells and enable tumor cells to escape host immunity. Comparison of the methylome of the two tumor models provided clues to a methyl metabolism shift during tumor progression that may be summarized as follows. Early stages of tumorigenesis could be characterized by global histone methylation as a means of genome protection or regulation. Subsequent stages of tumor development require increased gene transcription, and thus chromatin remodeling to make DNA more accessible, including histone demethylation. This may be achieved by competition of cytoplasmic methyltransferases with epigenetic methyltransferases for methyl groups and activation of demethylases. Although these mechanisms may fully explain findings in B16 melanoma models, it remains to ensure that the in vivo tumor methylome was not partly imported from the blood.

■ ASSOCIATED CONTENT

Supporting Information

The Supporting Information is available free of charge at https://pubs.acs.org/doi/10.1021/acs.jproteome.1c00778.

Figure S1, showing an HSQC spectrum of a [^{13}C-*methyl*]Met-labeled B16 melanoma tumor displaying a cysteine signal (PDF)

Special Issue Paper

This paper was intended for the Metabolomics Research Special Issue, published as the March 4, 2022 issue of *J. Proteome Res.* (Vol. 21, No. 3).

■ AUTHOR INFORMATION

Corresponding Author

Daniel Morvan − *UCA University, 63001 Clermont-Ferrand, France; Comprehensive Cancer Centre Jean Perrin, 63011 Clermont-Ferrand, France;* orcid.org/0000-0001-5473-7321; Phone: +33 473177900; Email: daniel.morvan@uca.fr

Author

Florent Cachin − *UCA University, 63001 Clermont-Ferrand, France; Comprehensive Cancer Centre Jean Perrin, 63011 Clermont-Ferrand, France; Inserm UMR 1240 IMOST, 63011 Clermont-Ferrand, France*

Complete contact information is available at: https://pubs.acs.org/10.1021/acs.jproteome.1c00778

Author Contributions

#D.M. and F.C. contributed equally.

Notes

The authors declare no competing financial interest.

■ ABBREVIATIONS

HRMAS, high-resolution magic angle spinning; HSQC, heteronuclear single quantum coherence; CPV, cross-peak volume; OPLS-DA, orthogonal partial least squares discriminant analysis

■ REFERENCES

(1) DeBerardinis, R. J.; Lum, J. J.; Hatzivassiliou, G.; Thompson, C. B. The Biology of Cancer: Metabolic Reprogramming Fuels Cell Growth and Proliferation. *Cell Metabolism* **2008**, *7* (1), 11−20.

(2) Saghafinia, S.; Mina, M.; Riggi, N.; Hanahan, D.; Ciriello, G. Pan-Cancer Landscape of Aberrant DNA Methylation across Human Tumors. *Cell Reports* **2018**, *25* (4), 1066−1080.e8.

(3) Ehrlich, M. DNA Hypomethylation in Cancer Cells. *Epigenomics* **2009**, *1* (2), 239−259.

(4) Esteller, M. Epigenetic Gene Silencing in Cancer: The DNA Hypermethylome. *Hum. Mol. Genet.* **2007**, *16* (R1), R50−R59.

(5) Mentch, S. J.; Mehrmohamadi, M.; Huang, L.; Liu, X.; Gupta, D.; Mattocks, D.; Gómez Padilla, P.; Ables, G.; Bamman, M. M.; Thalacker-Mercer, A. E.; Nichenametla, S. N.; Locasale, J. W. Histone Methylation Dynamics and Gene Regulation Occur through the Sensing of One-Carbon Metabolism. *Cell Metabolism* **2015**, *22* (5), 861−873.

(6) Kim, Y.-I. Nutritional Epigenetics: Impact of Folate Deficiency on DNA Methylation and Colon Cancer Susceptibility. *Journal of Nutrition* **2005**, *135* (11), 2703−2709.

(7) Ulanovskaya, O. A.; Zuhl, A. M.; Cravatt, B. F. NNMT Promotes Epigenetic Remodeling in Cancer by Creating a Metabolic Methylation Sink. *Nat. Chem. Biol.* **2013**, *9* (5), 300−306.

(8) Martínez-Chantar, M. L.; Vázquez-Chantada, M.; Ariz, U.; Martínez, N.; Varela, M.; Luka, Z.; Capdevila, A.; Rodríguez, J.; Aransay, A. M.; Matthiesen, R.; Yang, H.; Calvisi, D. F.; Esteller, M.; Fraga, M.; Lu, S. C.; Wagner, C.; Mato, J. M. Loss of the Glycine N-Methyltransferase Gene Leads to Steatosis and Hepatocellular Carcinoma in Mice. *Hepatology* **2008**, *47* (4), 1191−1199.

(9) Ye, C.; Sutter, B. M.; Wang, Y.; Kuang, Z.; Tu, B. P. A Metabolic Function for Phospholipid and Histone Methylation. *Mol. Cell* **2017**, *66* (2), 180−193.e8.

(10) Mudd, S. H.; Brosnan, J. T.; Brosnan, M. E.; Jacobs, R. L.; Stabler, S. P.; Allen, R. H.; Vance, D. E.; Wagner, C. Methyl Balance and Transmethylation Fluxes in Humans. *American Journal of Clinical Nutrition* **2007**, *85* (1), 19−25.
(11) Tang, H.; Tian, B.; Brasier, A. R.; Sowers, L. C.; Zhang, K. Measurement of Histone Methylation Dynamics by One-Carbon Metabolic Isotope Labeling and High-Energy Collisional Dissociation Methylation Signature Ion Detection. *Sci. Rep* **2016**, *6*, 31537.
(12) Zee, B. M.; Levin, R. S.; Xu, B.; LeRoy, G.; Wingreen, N. S.; Garcia, B. A. In Vivo Residue-Specific Histone Methylation Dynamics. *J. Biol. Chem.* **2010**, *285* (5), 3341−3350.
(13) Herring, J. L.; Rogstad, D. K.; Sowers, L. C. Enzymatic Methylation of DNA in Cultured Human Cells Studied by Stable Isotope Incorporation and Mass Spectrometry. *Chem. Res. Toxicol.* **2009**, *22* (6), 1060−1068.
(14) Theillet, F.-X.; Liokatis, S.; Jost, J. O.; Bekei, B.; Rose, H. M.; Binolfi, A.; Schwarzer, D.; Selenko, P. Site-Specific Mapping and Time-Resolved Monitoring of Lysine Methylation by High-Resolution NMR Spectroscopy. *J. Am. Chem. Soc.* **2012**, *134* (18), 7616−7619.
(15) Abramov, G.; Velyvis, A.; Rennella, E.; Wong, L. E.; Kay, L. E. A Methyl-TROSY Approach for NMR Studies of High-Molecular-Weight DNA with Application to the Nucleosome Core Particle. *Proc. Natl. Acad. Sci. U. S. A.* **2020**, *117* (23), 12836−12846.
(16) Saborano, R.; Eraslan, Z.; Roberts, J.; Khanim, F. L.; Lalor, P. F.; Reed, M. A. C.; Günther, U. L. A Framework for Tracer-Based Metabolism in Mammalian Cells by NMR. *Sci. Rep* **2019**, *9* (1), 2520.
(17) Bayet-Robert, M.; Loiseau, D.; Rio, P.; Demidem, A.; Barthomeuf, C.; Stepien, G.; Morvan, D. Quantitative Two-Dimensional HRMAS ^{1}H-NMR Spectroscopy-Based Metabolite Profiling of Human Cancer Cell Lines and Response to Chemotherapy. *Magn. Reson. Med.* **2010**, *63* (5), 1172−1183.
(18) Mao, J.; Jiang, L.; Jiang, B.; Liu, M.; Mao, X. A Selective NMR Method for Detecting Choline Containing Compounds in Liver Tissue: The ^{1}H-^{14}N HSQC Experiment. *J. Am. Chem. Soc.* **2010**, *132* (49), 17349−17351.
(19) Jofre, F.; Anderson, M. E.; Markley, J. L.; Rapolu, R. Tetramethylammonium. *BMRB Data Bank*, 2010. DOI: 10.13018/BMSE000780
(20) Liebeke, M.; Bundy, J. G. Biochemical Diversity of Betaines in Earthworms. *Biochem. Biophys. Res. Commun.* **2013**, *430* (4), 1306−1311.
(21) Griffith, C. M.; Williams, P. B.; Tinoco, L. W.; Dinges, M. M.; Wang, Y.; Larive, C. K. ^{1}H NMR Metabolic Profiling of Earthworm (Eisenia Fetida) Coelomic Fluid, Coelomocytes, and Tissue: Identification of a New Metabolite-Malylglutamate. *J. Proteome Res.* **2017**, *16* (9), 3407−3418.
(22) Goldberg, Y.; Ābele, E.; Bremanis, G.; Trapenciers, P.; Gaukhman, A.; Popelis, J.; Gomtsyan, A.; Kalviņš, I.; Shymanska, M.; Lukevics, E. Betaines Derived from Amino and Hydrazino Acids as Phase Transfer Catalysts. *Tetrahedron* **1990**, *46* (6), 1911−1922.
(23) Kimura, C.; Nukina, M.; Igarashi, K.; Sugawara, Y. *β*-Hydroxyergothioneine, a New Ergothioneine Derivative from the Mushroom Lyophyllum Connatum, and Its Protective Activity against Carbon Tetrachloride-Induced Injury in Primary Culture Hepatocytes. *Biosci., Biotechnol., Biochem.* **2005**, *69* (2), 357−363.
(24) Rae, C. D.; Sweeney, K. J.; Kuchel, P. W. Stability and Nonreactivity of Ergothioneine in Human Erythrocytes Studied by ^{1}H NMR. *Magn Reson Med.* **1993**, *29* (6), 826−829.
(25) Choudhury, M. K.; Eichenberger, W. Synthesis of Betaine Lipids: Dipropionylglyceryl(N,N,N-Trimethyl)Serine. *Chem. Phys. Lipids* **1985**, *36* (4), 351−359.
(26) *Human Metabolome Database: Showing metabocard for Taurine (HMDB0000251)* https://hmdb.ca/metabolites/HMDB0000251 (accessed 2021-05-03).
(27) Brand, A.; Leibfritz, D.; Hamprecht, B.; Dringen, R. Metabolism of Cysteine in Astroglial Cells: Synthesis of Hypotaurine and Taurine. *Journal of Neurochemistry* **1998**, *71* (2), 827−832.
(28) *KEGG PATHWAY: Cysteine and methionine metabolism - Mus musculus (mouse)*. https://www.genome.jp/kegg-bin/show_pathway?mmu00270 (accessed 2021-05-03).
(29) Gao, M.; Nadaud, P. S.; Bernier, M. W.; North, J. A.; Hammel, P. C.; Poirier, M. G.; Jaroniec, C. P. Histone H3 and H4 N-Terminal Tails in Nucleosome Arrays at Cellular Concentrations Probed by Magic Angle Spinning NMR Spectroscopy. *J. Am. Chem. Soc.* **2013**, *135* (41), 15278−15281.
(30) Ye, C.; Tu, B. P. Sink into the Epigenome: Histones as Repositories That Influence Cellular Metabolism. *Trends Endocrinol Metab* **2018**, *29* (9), 626−637.
(31) Lu, C.; Thompson, C. B. Metabolic Regulation of Epigenetics. *Cell Metab.* **2012**, *16* (1), 9−17.
(32) Park, G. H. J.; Yang, S.-H.; Baek, H.-M. 900 MHz ^{1}H-/^{13}C-NMR Analysis of 2-Hydroxyglutarate and Other Brain Metabolites in Human Brain Tumor Tissue Extracts. *PLoS One* **2018**, *13* (9), No. e0203379.
(33) Webb, K. J.; Lipson, R. S.; Al-Hadid, Q.; Whitelegge, J. P.; Clarke, S. G. Identification of Protein N-Terminal Methyltransferases in Yeast and Humans. *Biochemistry* **2010**, *49* (25), 5225−5235.
(34) Burgos-Barragan, G.; Wit, N.; Meiser, J.; Dingler, F. A.; Pietzke, M.; Mulderrig, L.; Pontel, L. B.; Rosado, I. V.; Brewer, T. F.; Cordell, R. L.; Monks, P. S.; Chang, C. J.; Vazquez, A.; Patel, K. J. Mammals Divert Endogenous Genotoxic Formaldehyde into One-Carbon Metabolism. *Nature* **2017**, *548* (7669), 549−554.
(35) Heger, Z.; Rodrigo, M. A. M.; Michalek, P.; Polanska, H.; Masarik, M.; Vit, V.; Plevova, M.; Pacik, D.; Eckschlager, T.; Stiborova, M.; Adam, V. Sarcosine Up-Regulates Expression of Genes Involved in Cell Cycle Progression of Metastatic Models of Prostate Cancer. *PLoS One* **2016**, *11* (11), No. e0165830.
(36) Musich, J. A.; Rapoport, H. Reaction of O-Methyl-N,N'-Diisopropylisourea with Amino Acids and Amines. *J. Org. Chem.* **1977**, *42* (1), 139−141.
(37) Khan, A.; Leśniak, R. K.; Brem, J.; Rydzik, A. M.; Choi, H.; Leung, I. K. H.; McDonough, M. A.; Schofield, C. J.; Claridge, T. D. W. Development and Application of Ligand-Based NMR Screening Assays for *γ*-Butyrobetaine Hydroxylase. *MedChemComm* **2016**, *7* (5), 873−880.
(38) Agostini, G.; Coletta, F.; Gambaro, A.; Castellano, S. 1H and 13C NMR Studies on DL-Carnitine Hydrochloride in D_2O. *Spectrochimica Acta Part A: Molecular Spectroscopy* **1979**, *35* (7), 733−737.
(39) Hertzberg, T.; Kühler, T.; Nilsson, M.; Enzell, C. R.; Berg, J.-E.; Ljungqvist, A. Preparation of (S)-5-Amino-5-Carboxy-N,N,N-Trimethyl-1-Pentaneaminium Chloride (L-Lysinebetaine Hydrochloride). *Acta Chem. Scand.* **1986**, *40b*, 387−389.
(40) Al Temimi, A. H. K.; Pieters, B. J. G. E.; Reddy, Y. V.; White, P. B.; Mecinović, J. Substrate Scope for Trimethyllysine Hydroxylase Catalysis. *Chem. Commun. (Camb)* **2016**, *52* (87), 12849−12852.
(41) Blunden, G.; Gordon, S. M.; Crabb, T. A.; Roch, O. G.; Rowan, M. G.; Wood, B. NMR Spectra of Betaines from Marine Algae. *Magn. Reson. Chem.* **1986**, *24* (11), 965−971.
(42) Henry, G. D.; Dalgarno, D. C.; Marcus, G.; Scott, M.; Levine, B. A.; Trayer, I. P. The Occurrence of Alpha-N-Trimethylalanine as the N-Terminal Amino Acid of Some Myosin Light Chains. *FEBS Lett.* **1982**, *144* (1), 11−15.
(43) Phalaraksh, C.; Lenz, E. M.; Lindon, J. C.; Nicholson, J. K.; Farrant, R. D.; Reynolds, S. E.; Wilson, I. D.; Osborn, D.; Weeks, J. M. NMR Spectroscopic Studies on the Haemolymph of the Tobacco Hornworm, Manduca Sexta: Assignment of ^{1}H and ^{13}C NMR Spectra. *Insect Biochem. Mol. Biol.* **1999**, *29* (9), 795−805.

https://doi.org/10.1021/acs.jproteome.1c00778
J. Proteome Res. 2022, 21, 940−952